LAWRENCE
LIVERMORE
NATIONAL
LABORATORY

UCRL-JRNL-207273

Identification of minerals and meteoritic materials via Raman techniques after capture in hypervelocity impacts on aerogel

M. J. Burchell, J. Mann, J. A. Creighton, A.T. Kearsley, G. A. Graham, A. P. Esposito, I. A. Franchi, A. J. Westphal, C. Snead

October 15, 2004

Meteoritic and Planetary Science

Identification of Minerals and Meteoritic Materials Via Raman Techniques After Capture in Hypervelocity Impacts on Aerogel

M.J. Burchell[1], J. Mann[1], J.A. Creighton[1], A.T. Kearsley[2], G. Graham[3], A.P. Esposito[3], I. A. Franchi[4] and A.J. Westphal[5] and C. Snead[5]

[1]Centre for Astrophysics and Planetary Sciences, School of Physical Sciences, University of Kent, Canterbury, Kent CT2 7NR, United Kingdom

[2] Department of Mineralogy, The Natural History Museum, Cromwell Road, London SW7 5BD, United Kingdom.

[3] Lawrence Livermore National Laboratory, Livermore, California 94551, United States of America.

[4] Planetary and Space Science Research Institute, The Open University, Milton Keynes MK7 6AA, United Kingdom

[5]Space Sciences Laboratory, University of California at Berkeley, Berkeley, California 94720, United States of America.

Contact person:
Dr. M.J. Burchell,
Centre for Astrophysics and Planetary Sciences
School of Physical Sciences
University of Kent
Canterbury
Kent CT2 7NR
United Kingdom
Email: : M.J.Burchell@kent.ac.uk

Abstract:

For this study, an extensive suite of mineral particles analogous to components of cosmic dust were tested to determine if their Raman signatures can be recognised after hypervelocity capture in aerogel. The mineral particles were mainly of greater than 20 micrometres in size and were accelerated onto the silica aerogel by light gas gun shots. It was found that all the individual minerals captured in aerogel could be subsequently identified using Raman (or fluorescent) spectra. The beam spot size used for the laser illumination was of the order of 5 micrometres, and in some cases the captured particles were of a similar small size. In some samples fired into aerogel there was observed a shift in the wavenumbers of some of the Raman bands, a result of the trapped particles being at quite high temperatures due to heating by the laser. Temperatures of samples under laser illumination were estimated from the relative intensities of Stokes and anti-Stokes Raman bands, or, in the case of ruby particles, from the wavenumber of fluorescence bands excited by the laser. It was found that the temperature of particles in aerogel varied greatly, dependent upon laser power and the nature of the particle. In the worst case, some particles were shown to have temperatures in the 500-700 °C range at a laser power of about 3 mW at the sample. However most of the mineral particles examined at this laser power had temperatures below 200 °C. This is sufficiently low a temperature not to damage most materials expected to be found captured in aerogel in space. In addition, selected meteorite samples were examined to obtain Raman signatures of their constituent minerals and were then shot into aerogel. It was possible to find several Raman signatures after capture in aerogel and obtain a Raman map of a whole grain in situ in the aerogel. Finally, a Raman analysis was carried out of a particle captured in aerogel in space and carbonaceous material identified. In general therefore it is concluded that Raman analysis is indeed well suited for an in-situ analysis of micrometre sized non-terrestrial materials captured in aerogel.

Introduction

Raman spectroscopy is a well-established method for identifying substances, and recent instrumental developments, notably the integration of Raman spectrometers with confocal microscopes and the introduction of ultra-sensitive CCD detectors, have made this an effective technique for chemically characterising small particles or inhomogeneous solids. In essence, Raman spectroscopy involves measurement of the spectrum of the scattered light when a substance is illuminated by a monochromatic light source, typically a laser. Although most of the scattered light is of unchanged frequency, inelastic scattering produces side-bands on the laser line, due to the exchange of energy with vibrations of the chemical bonds of the sample. The frequency shifts from the laser line are the bond vibration frequencies, and thus the Raman spectrum is a vibrational spectrum, giving a highly characteristic fingerprint of the chemical nature of the sample. Chemical identification may be made by matching the spectrum with a database of standard spectra, or the individual bands in the Raman spectrum may be used to infer the presence of particular bonds in the sample by reference to tables of characteristic bond vibration frequencies.

As an analytical technique, Raman spectroscopy has the attractive feature that it may be applied to substances as presented, without prior sample preparation, and it is usually non-destructive of the sample. For some samples (as is the case for impure alumina samples discussed below), illumination by the laser may also excite fluorescence, and the fluorescence bands may lie in the same spectra region as the Raman spectrum, superimposed on the much weaker Raman bands. In contrast to the light scattering inherent in Raman spectroscopy, fluorescence involves the absorption of photons due to electronic transitions in the sample, and the subsequent re-emission of frequency-shifted photons. Fluorescence spectra are thus electronic emission spectra, and fluorescence is restricted to samples which absorb at the laser wavelength.

Raman scattering is thus well suited to identifying unknown materials. Lasers (either visual wavelengths or infra red for example) can provide the incident radiation and efficient, narrow band filters can remove the elastically scattered light. Raman systems are typically incorporated into microscopes, so samples can be optically imaged, sites chosen for study and Raman spectra obtained. The spectra can be compared to a database and the sample composition obtained. The spot size for the illumination can be of order 10 microns or less, and may approach the micrometer scale in modern confocal optical systems. Thus non-homogeneous materials can have their content studied at such scales.

Since the 1960's Raman spectroscopy has increasingly been used as a characterisation method by mineralogists, and there are also several applications of Raman techniques to planetary science. For example, Wopenka, 1988, used Raman to study interplanetary dust particles collected in the atmosphere. Meteorite samples have also been studied (e.g. Michel-Levy and Lautie, 1981, Wopenka and Sandford, 1984, Heymann, 1987), looking at mineral phases or the presence of carbon. In addition, Martian meteorites have been studied (e.g. Wang *et al*., 1999) along with the suggestion that a micro-Raman system be deployed remotely on Mars for in-situ analysis of minerals. This idea has been developed further by Wynn-Williams and Edwards, 2000, who reported that infra-red Raman can be used to identify biomolecules (via their pigment and photoprotective mineral contents) in the Antarctic and who also suggested using such a system on Mars to find regolith habitats on that planet. More recently Popp *et al*., 2002, studied meteorite samples with a range of surface textures. They typically found that 85% of Raman spectra obtained could be assigned to a certain mineral, and that in the worst (most heavily textured) case 60% of spectra could still be assigned to known minerals. The advantage of an analytical tool that requires minimal sample handling and preparation (and hence negligible modification or contamination) whilst providing subtle mineral characterisation is obvious, and it holds particular promise for initial non-invasive examination of valuable extraterrestrial samples such as those returned by sample return missions to asteroids (e.g. NEO 1998SF36 to be visited by MUSES-

C/Hayabusa, see Kawaguchi *et al*., 2003 and Fujiwara *et al*., 1999 and 2004) and comets (e.g. the Stardust encounter with P-Wild2, see Brownlee *et al*., 1996 and 2003).

Recently a new method of collecting samples of extraterrestrial materials has been deployed in space, namely the use of aerogel to capture small dust particles which impact at high speeds, typically many km s^{-1}. Tsou *et al*., 1988 showed that despite high impact speeds which normally cause vaporisation of the particles when they hit a solid, for impacts at several km s^{-1} into aerogel the particles are captured relatively intact. Our early results on the location of impacted mineral grains by analytical electron microscopy and laser confocal imagery (ref. Graham *et al*., 2004) have shown that particles may fragment during penetration, leaving smaller debris scattered along the characteristic impact track. This is in stark contrast to impacts on normal 'solids' such as metal or glass, in which little solid material survives, and residues are restricted to melt and vapour condensates (Graham *et al*., 2001a). The key is that aerogel is a highly porous, low-density material (essentially a dried silica gel). The result of the low density (which can be made less than 20 kg m^{-3}) is that in an impact the impactor tunnels into the aerogel target and is slowed relatively gently. The captured particle is thus often found at the end of a relatively long, carrot shaped track. Since aerogel is transparent, the track and captured particle are easily seen. Several experiments have deployed aerogel capture cells in space and impacts of small (typically less than 100 or even 10 micron) particles reported (e.g. Brownlee *et al*, 1994, Burchell *et al*., 1999a, Hörz *et al*., 2000). In addition, the NASA Stardust spacecraft (Brownlee *et al*., 2003) was launched in 1999 to visit a comet in 2004 and capture freshly emitted dust grains in aerogel, at a relative encounter velocity of 6.1 km s^{-1} (Tsou *et al*., 2003). These will be returned to Earth in 2006.

Appropriate analysis techniques need to be applied to the samples captured in aerogel after their return to Earth. For example, Flynn *et al*., 1996 showed that synchrotron radiation could provide the elemental composition of captured grains. Subsequently, Burchell *et al*., 2001 showed that Raman techniques could be successfully applied to particles of several types of minerals fired into aerogel in the laboratory at ≈5 km s^{-1}. They demonstrated that this worked for olivine and enstatite, whilst ruby and spinel particles gave strong fluorescence signals that were also characteristic of these minerals after capture in aerogel. This Raman analysis is in-situ, so obviates the need for removing the captured particles from the aerogel. Subsequently, Graham *et al*., 2001b showed that grains of Allende meteorite could be fired into aerogel at 5 km s^{-1} and Raman spectra obtained which allowed the identification of olivine and carbonaceous components. Recently, Burchell *et al*., 2004 have shown that complex organic materials can be fired into aerogel at 5 km s^{-1} and still be identified by their Raman signatures

Clearly, Raman is a technique that works with at least some mineral and organic materials captured in aerogel at high speed. However, there are many open questions. What sort of range of mineral materials can be studied in aerogel with Raman? Are any important mineral species difficult or impossible to identify by Raman techniques, and what are the best operating conditions for reliable mineral identification? Do any minerals show changes in their Raman spectra as a result of the capture process? How well can different mineral components be identified in inhomogeneous particles, especially when intimately mingled? And what is the degree of heating inherent in laser illumination during a Raman study of particles captured in aerogel? In this paper we attempt to investigate, discuss and resolve these issues. We have fired a wide range of minerals into aerogel, we report on the effect of laser illumination on the temperature of the captured samples, and have also shot in-homogeneous meteorite samples into aerogel.

Method

The main tools for the work reported herein are a two-stage light gas gun (to achieve high speed impacts in the laboratory) and a Raman system. The two-stage gun that was used is described in

Burchell *et al*., 1999b. Such guns use a gunpowder charge to drive a piston. This is used to compress a light gas. The sudden release of the light gas (via rupture of a thin containing disk of metal) is used to accelerate the real projectile, which in this case was mounted in a sabot (which was discarded in flight). The speed of the shot can be selected by adjusting the amount of gunpowder, composition and pressure of the light gas, etc. In flight the projectiles travel through the range of the gun that is maintained at a low pressure of less than 1 mbar to prevent slowing of the projectiles in flight due to air resistance. The projectile used in a shot could be a single, mm sized particle, or a number of grains of a material (typically 10 or 20 particles, each a few tens to hundred microns in size). The speed of the shot is found from signals given by passage of the projectiles through two laser light curtains, combined with signals from impact sensors mounted on the stop plate which intercepts the discarded sabot and the target holder. The timing information from these signals, combined with the locations of the measurement points, gives the speed in each shot, accurate to ±4%.

The aerogel used in this work had a density of 60, 96 or 110 kg m^{-3}. Long, thin slabs (5 cm length, 1 cm x 2 cm end face) were mounted 'end-on' in a target holder (two or three slabs per shot). Typically 5 to 10 particles per shot would hit the aerogel (i.e. 2 or 3 per slab). The tracks (Figure 1) could easily be viewed through the side of the slabs and examined under a microscope system to show the captured particles. The Raman system used at the University of Kent comprised a Jobin Yvon micro-Raman module combined with an Olympus BX40 microscope. This was coupled to a model HR640 spectrograph with liquid nitrogen cooled CCD. Illumination was from a He-Ne laser (632.8 nm) which gave about 3 mW of power at the sample, and the measurements were made using a ×50 long working distance objective which gave a focused laser spot of diameter 5 μm. Raman mapping was performed at the Open University on a Jobin-Yvon LabRaman spectrometer coupled to a microscope, utilising an Ar^+ ion (514 nm) laser, and Raman mapping software giving automated raster scanning of the sample. The Raman spectra were obtained from a sample volume of approximately 2 micrometres diameter by 2 micrometres depth by use of an objective of ×50 magnification. Fluorescence imaging and Raman spectral analysis were preformed at Lawrence Livermore National Laboratory using an inverted optical microscope (Zeiss Axiovert S100 TV). Positioning of the sample was achieved by a closed-loop, xy piezo stage (Physik Instrumente), which is controlled using commercially available electronics and software (Digital Instruments Nanoscope IIIa). Excitation for the fluorescence imaging and Raman scattering was provided by the 488 nm line of an Ar^+ laser (Coherent Innova 70).

Mineral Categorisation

Previously, with the same instrumentation as above, it had been shown (Burchell *et al*, 2001) that olivine and enstatite grains gave recognisable Raman spectra after capture in aerogel at ≈5 km s^{-1}. In addition, spinel and corundum (ruby) gave fluorescent signals that could also be used to identify those particles. In the present work seven more minerals were investigated, in addition to further study of the previous four. Details of all the minerals are given in Table 1, along with examples of the general class of meteorites in which they have been observed (and in some cases examples of specific meteorites known to contain them). Thus a wide range of minerals found in meteoritic materials has been tested.

In each case Raman spectra of the raw grains were first obtained. For confirmation, these were compared to a standard database of Raman spectra (http://minerals.gps.caltech.edu/FILES/raman/Index.htm and links therein). Samples of each material were then fired into the aerogel of density 60 - 110 kg m^{-3} (aerogel densities and impact speeds as given in Table 1). Capture was successful in all cases except for the hydrous phyllosilicate serpentine. Despite several attempts, no particles of serpentine were found to have reached the target (i.e. no tracks were observed in the aerogel and no speed was obtained). It seems that the serpentine particles disintegrated under the shock of acceleration into much smaller

particles, possibly of sub-micron size (note that the buck-shot technique has proven effective in delivering grains as small as three microns onto other targets in the gun at Kent). Consistent with this is the observation that in the case of calcite some of the captured particles in the aerogel were found to be of only 5 to 10 microns in size despite the fact that the initial mineral projectiles were fired as mixtures of 50 to 100 micron grains. This again suggests that substantial grain fragmentation occurred during the shot, probably as a function of the very well developed crystal lattice cleavage that is so characteristic of this mineral. Such fragmentation problem has also been observed in previous shots of calcium carbonate onto solar cell glass. Nevertheless, the small particles in aerogel still gave recognisable Raman spectra. Separately, we note that recent experimental evidence strongly suggests that, for example, carbonate minerals (such as calcite) do not undergo substantial dissociation and loss of carbon dioxide even at the peak shock pressures experienced during hypervelocity impact (Jones *et al*., 2000).

For all the minerals captured in the aerogel in-situ Raman or fluorescence spectra were obtained which were sufficient for mineral identification. The Raman spectra for the raw grains and for the grains trapped in aerogel are shown in Figure 2. In each comparison the spectra are clearly similar. Thus for a wide range of minerals, the capture process in aerogel has neither obscured nor so significantly altered the spectra as to make them unrecognisable. It is particularly significant that such important information can be obtained from impacts into relatively high aerogel density (110 kg m^{-3}), and encouraging for survival of material impacting into lower density aerogel such as that on the Stardust spacecraft (20 kg m^{-3}).

In addition to the minerals in Table 1 characterised by their Raman spectra, two other materials were also studied, namely alumina and spinel, for which the bands measured with the Raman spectrometer were due to fluorescence rather than to Raman scattering. For both these substances the fluorescence is due to Cr^{3+} ions, thus showing the presence of Cr^{3+} as an impurity in the alumina samples, and as with the Raman spectra the fluorescence spectra are sufficiently sharp to be of fingerprint value for recognising these substances, as shown in Figure 3. (Note that, as is conventional for emission spectra, the fluorescence spectra in Figures 3, 4 and 11 are shown with an absolute wavenumber scale, rather than with a wavenumber shift scale as is conventional for Raman spectra). Alumina is of interest here since fine aluminium powder is a major component of solid rocket motor fuel and produces small Al_2O_3 particles in the rocket's exhaust. Thus large numbers of micron sized alumina particles are regularly injected into Earth orbit from spacecraft rocket engines, and can be expected to feature in any aerogel sample exposed in Earth orbit. Although the alumina powder used in our shots was from a single source of synthetic alumina, an examination of the raw grains (and those in the aerogel) also found evidence for some grains with different fluorescent spectra. These are shown in Figure 4 (where the lower spectra is the one most commonly found and the upper two are the variants). No explanation was found for this diversity in the single source of alumina, but major differences in colour of natural alumina grains can be explained by minor variation in the content of first row transition elements. Similarly, in the case of the spinel samples, what was originally thought to be a homogeneous sample of natural red spinel grains from an alluvial placer deposit, subsequently revealed two quite distinct fluorescence spectra (one the ruby fluorescence) from different grains. Detailed compositional analysis of grains in a sample of the projectile powder showed that prior to mineral crushing and sieving, some ruby grains (a red form of natural corundum, impure alumina) had been mistaken for red spinels, and incorporated into the sample, and had contaminated an otherwise homogeneous mineral sample. The standard spectra for alumina and spinel are those shown in Figure 3. The distinction between these two mineral species was also clear after their capture in aerogel.

Silicon carbide was also examined as part of this study because grains of this composition have been reported in primitive unequilibrated chondritic meteorites (Bernatowicz *et al*., 1987), and are believed to be survivors from the proto-Solar nebula. They may also be present as

individual discrete grains amongst the population of Interstellar Dust particles (ISP). Presolar SiC grains may carry trace element isotopic signatures that demonstrate their environment of origin and are characteristic of specific nucleosynthetic processes (Amari *et al*., 2001). They may be vulnerable to destruction through oxidation during many processes of meteoritic equilibration at elevated temperatures and in the presence of reactive volatiles. It is not yet known whether silicon carbide is present within cometary particles, although the postulated lack of post-nebular alteration events in smaller icy bodies (few km diameter) accreted outside 20 AU may suggest their likely survival. Again, shots into aerogel were carried out at 5 km s^{-1}. The Raman spectra from the raw materials and the particles captured in aerogel are shown in Figure 5. There is good agreement between the spectra of the raw particles and those taken in-situ after capture in aerogel. The recognition of SiC grains within undisturbed aerogel by a relatively non-invasive and contamination-free technique is potentially very important. It will allow location of individual grains and their careful physical preparation, using techniques such as those of Westphal *et al*. (2002) prior to trace element isotopic analysis without grain damage or contamination.

The majority of projectiles investigated in our study were of single mineral crystals, or were relatively strong fragments of carbonaceous chondrite meteorite (see below), both of which may penetrate aerogel deeply, leaving an obvious discrete particle remnant near the terminal point of the track. It is possible that delicate 'fluffy' particles, which appear in interplanetary dust collections and which may dominate fresh cometary dust (Greenberg and Hage, 1990), will be even more prone to disintegration during capture. In which case the aerogel tracks may contain micron sized (or smaller) debris along the track rather than a relatively large captured grain at the end. In such cases, a Raman analysis of the debris along the length of a track should be attempted as well as of any fragment at the end of a track. In general Raman techniques do work on sub-micron sized objects, although the smallest objects identified here were approximately 3 microns across.

It thus seems clear from the minerals studied that the potential for use of Raman analysis after hypervelocity capture in aerogel is not limited to just a few minerals. Indeed, all the materials successfully fired into aerogel gave recognisable signals afterward (either Raman shift spectra or fluorescent spectra). It is clear that this type of analysis can be used to search for a wide range of interesting materials captured in aerogel.

Meteorite Samples

Having demonstrated that hypervelocity capture in aerogel is not *a priori* destructive of the characteristic Raman signal from minerals, the next step in the work was to investigate capture in aerogel of particles of mixed composition and to attempt to identify their compositions using Raman techniques. Since study of extraterrestrial materials is the purpose of dust collection in space, meteoritic samples were used as analogues of one likely major source of interplanetary dust, Main Belt asteroids of the spectroscopic C-type (Gaffey, 1999). The meteorite samples chosen were the carbonaceous chondrites: Orgueil (CI, type 1, dominated by hydrous phyllosilicates, iron sulphide and iron oxide grains); Murchison (CM, type 2, with a fine-grained matrix bearing hydrous phyllosilicates and with well defined chondrules dominated by anhydrous mafic silicates, olivine and pyroxene) and Allende (CV, type 3 oxidised, with a fine-grained anhydrous silicate matrix, abundant mafic silicate chondrules and refractory inclusions rich in aluminium and calcium). Each meteorite is well documented and is demonstrably inhomogeneous in composition at the scale of a few micrometres. Although it is not yet possible to state precise proportions of mineral components in dust of cometary origin, and it is possible that much silicate material may be present as glass formed by prolonged exposure to radiation prior to icy body accumulation (Bradley, 2003), it is likely that olivine and pyroxene will also be present as discrete mineral phases (Crovisier *et al*. 1997)

This work proceeded in two phases. Firstly, 3 to 5 raw grains of each meteorite were studied under the Raman system. Spectra which only displayed the peaks characteristic of carbon (e.g. Figure 6, broad peaks at 1350 and 1594 cm^{-1}) were discarded and the remaining spectra were then compared to those we obtained for the standard terrestrial minerals in Table 1, or with the Raman spectra of minerals available on the database described above. Note that in doing this latter comparison, we make the assumption that since all the materials tested so far yielded similar Raman spectra before and after capture in aerogel, it was taken that this was true for all minerals with high dissociation temperatures. There is no proof of this but in the circumstances it is a useful and not unreasonable assertion. Matches were found which indicated the presence in the meteorite samples of the minerals listed in Table 2, and only one of the spectra remained un-matched after this process. Examples of the spectra showing the matches to standard spectra are given in Figure 7. The minerals detected include olivine, enstatite, calcic clinopyroxene, sulfur, and anatase, with the additional presence of amorphous carbon in some of the grains, as indicated by the superimposed broad peaks at 1350 and 1594 cm^{-1}. Only in one or two cases was the match ambiguous. Thus one spectrum could have been either dolomite or magnesite, which are closely related magnesium-bearing carbonate minerals, both known from carbonaceous chondrite meteorites. Another spectrum contained bands characteristic of sulphate ions superimposed on bands indicative of sulphur. On comparing with standard spectra available to us, these sulphate bands gave a better match to jarosite than to simple sulphates such as barite or anhydrite, though it is likely that there are other sulphate-containing minerals which would have given a similar match. In any case, caution is required before assigning the identified minerals as being part of the primordial body. For example, the presence of sulphur is anomalous, and may be related to the growth of sulfates which is known to occur rapidly after arrival on Earth (Gounelle and Zolensky, 2001) and possibly their reduction by microbial processes. From these results, it is clear that Raman techniques can be used to identify individual mineral grains in meteorite samples, confirming previous work (e.g. see Popp *et al.*, 2002 for a recent paper on the subject).

As the second part of the experiment, samples of each meteorite were fired into aerogel (density 110 kg m^{-3}) at 5.0 to 5.6 km s^{-1}. Despite attempts on half a dozen grains, no strong spectra were obtained from the Murchison samples. The best that was found were spectra with hints of olivine peaks and the bands indicative of carbon. By contrast, good spectra were obtained from specific locations on the captured grains of Allende and Orgueil (examples are shown in Figure 8, displaying clear Raman lines attributable to olivine and pyroxine within the meteorite). Using the higher spatial resolution and the mapping capability of the Labram spectrometer, Raman maps of a depth-resolved slice through an entire Allende grain were also generated. This was achieved using the rastering method (also see Graham *et al.*, 2001b), with rapid point sampling (typically 6 seconds for a complete spectrum acquisition at each pixel point). At each pixel point a full spectrum is collected (typically from 0 to 2500 cm^{-1} shift) and is stored as a pristine data-set for further analysis after the map completion. To produce maps from the raw data-set, a range of spectrum background fitting and subtraction methods can be used. Individual pixel spectra, or the sum of all the spectra, are used to define wave number bounds between which the signal level is integrated to yield an intensity measurement. For each defined segment of the spectrum a grey-scale image of Raman line intensity can be generated, as shown in Figure 9. Thus the entire volume of a semitransparent grain encapsulated within aerogel can be analysed, and a map of mineral locations produced. Examples of maps from a grain of the Allende sample captured in aerogel are given in Figure 9. A green (514.5nm) laser was used with 7.7mW output, and the Raman signal was acquired through a x20 objective. In Figures 9b and 9c the characteristic peaks at 817 and 851 cm^{-1} were chosen to indicate the location of olivine. The differing intensities for the two lines are a function of the differing crystallographic lattice orientations in the two grains, generating polarisation contrast in the Raman line expression. In Figure 9d, 1590 cm^{-1} was chosen, indicative of carbon, demonstrating that this impacted grain contains both undamaged silicate

minerals and probably original meteoritic organic matter. The size of the grain (see in white light in Figure 9a) was 60 microns across, and the spot size (i.e. minimum potential spatial resolution in these maps) was approximately 3 microns.

Heating of Samples

One of the open issues with regard to use of Raman techniques on particles trapped in aerogel concerns the possibility of laser heating and consequent structural and chemical changes in the sample. In the Raman spectrometer the energy density at the focused laser spot is sufficiently high (ca. 100W mm^{-2}) for there to be the possibility of significant sample heating, and of particular concern is the efficiency of the aerogel in restricting heat dissipation from the particles. The degree of heating of small grains during Raman analysis has therefore been investigated.

Two methods have been employed. Firstly use has been made of the relative intensity of corresponding Raman bands on the low and high frequency sides (the Stokes and anti-Stokes sides) of the laser line. This intensity ratio is given by

$$R = \frac{I_{Antistokes}}{I_{Stokes}} = \left(\frac{\nu_0 + \nu}{\nu_0 - \nu}\right)^4 \exp\left(\frac{-h\nu c}{kT}\right) \quad , \qquad \text{Eqn 1}$$

where ν_0 is the wave-number of the incident light from the laser, ν is wavenumber shift for a particular Raman band, h is Planck's constant, c is the speed of light, k is Boltzmann's constant and T is the temperature. From the measured ratio R the temperature can therefore be obtained.

Raman bands on the anti-Stokes side were found to have fairly poor signal/noise ratio, particularly at large shifts from the laser line, and it was important that a curve-fitting package was used to measure the peak heights. Use was made of the package Peaksolve (Galactic Industries), and the bands were fitted to a mixed Gaussian Lorentzian or a Voigt band shape. It was also necessary to multiply the measured intensity ratios R by a correction factor to correct for the variation in spectrometer sensitivity across the spectrum. This factor was determined from measurements of R for several bands of the colourless liquids acetone, bromobenzene, tetrachloromethane and toluene. Since these liquids do not absorb at the laser wavelength, the correct value of the ratio R for each band could be calculated from eqn. 1 with T set equal to room temperature. The correction factor at the wavenumber of each band of these liquids was then the ratio of the calculated and measured values of R. Because of the difficulty of measuring the intensities of weak bands in the presence of noise, particularly on the anti-Stokes side, there was some spread in the temperatures obtained from different bands in the same spectrum, or from repeat scans. From this spread, the limits of accuracy of this method were estimated to be ±20° near room temperature, and ±60° near 500 °C.

Stokes/anti-Stokes Raman measurements were first carried out on various small (10 - 50 μm) particles in air on a microscope slide, and these showed that even in air there was significant heating of strongly absorbing particles. Thus for silicon carbide particles, which in bulk were dark grey, the temperature ranged from room temperature to 160 °C, with most of the particles in the range 100 to 160 °C. Olivine and calcite particles, however, which have low absorption at the laser wavelength, were found to be close to room temperature. The temperatures of particles of these substances in aerogel were found to be somewhat higher, respectively 180 (silicon carbide, Figure 10a), 20 (olivine) and 60 (calcite) °C, at this laser power. However a much higher temperature was recorded for a particle of an unknown impurity in the silicon carbide sample shot, which was also adventitiously fired into the aerogel, which reached 480 °C (Figure 10b, upper trace) in the focussed laser beam. The Raman spectrum of this particle with the laser attenuated to 10% of full power (giving a temperature of 75 °C) is shown in Figure 10b (lower trace). Not only are the bands on the anti-Stokes side more intense in the spectrum at the higher laser power, but also the band widths may be seen to be much greater at the higher power, clearly confirming the large difference in sample temperatures at the two laser powers. This illustrates how control of the

laser intensity can significantly change the temperature achieved by the illuminated particle. The basic principle should be to use the lowest illumination required to extract a spectrum. In this context it should be noted that heating to an equilibrium temperature occurs rapidly on time scales less than 1 s, and so for normal Raman integration times the magnitude of the heating depends on the power delivered rather than the duration of the illumination.

The second method that has been used to estimate the temperature of particles at the laser focus makes use of the fluorescence excited in ruby particles by the helium neon laser. This fluorescence consists of a pair of sharp emission bands near 14400 cm^{-1}, which thus lie in the same spectral region as Raman bands excited by the helium neon laser. The wavenumbers of these bands vary approximately linearly with temperature near 300 K with gradient -0.14 cm^{-1} K^{-1}, and their wavenumber shifts have been presented graphically up to 800 K (McCumber and Sturge, 1963). Interpolation of the measured fluorescence shifts in the published graphical data thus gives the temperature of ruby particles at the laser focus. Although confined to ruby particles, this method is of much greater accuracy for small changes in temperature than that based on Raman Stokes/anti-Stokes intensity ratios. Below 150 °C the band centres in the spectra could be measured to ±0.5 cm^{-1} by fitting a mixed Gaussian Lorenzian bandshape to the fluorescence bands, giving a temperature accuracy of ±4°. This accuracy is reduced above 150 °C because of broadening of the fluorescence bands towards higher temperatures.

Fluorescence measurements were first made on roughly 30 ruby particles in each of the size ranges ca. 50 μm and 5 - 10 μm in air on a microscope slide. The particles are of natural mineral origin, and are therefore not expected to be homogeneous in composition. No shift from the room temperature fluorescence wavenumber was found for any of the larger particles, or for well over half of smaller particles, and for ca. 20% of the smaller particles the shifts were 5 cm^{-1} or less (temperatures in the range 20 – 56 °C). For one particle (8 μm diam.), however, the shift was 55 cm^{-1}, corresponding to a temperature of 395 °C. In aerogel, heating effects were apparent, and of 15 ruby particles examined in aerogel almost all showed shifts in the fluorescence, giving temperatures fairly evenly distributed over the range 20 to 230 °C. However one particle of dimensions about 25 μm had a fluorescence shift of 96 cm^{-1}, showing that this particle was heated by the laser to ca. 700 °C. The fluorescence of this particle at the full laser power and at lower powers is shown in Figure 11. This clearly shows the change in temperature as the laser power is varied, but also of note is the sloping baseline which appears in the spectrum at full laser power, due to the black body emission of the particle at 700 °C.

It is clear from these observations that the extent of laser heating varies considerably for different particles. It is indeed greater for particles in aerogel than in air, but for the majority of samples in aerogel whose temperatures we have measured, temperatures did not exceed 200 °C. Thus for many mineral particles in aerogel at laser power densities comparable to our spectrometer, laser heating is likely to be insufficient to cause significant change. The measurements also show the expected reduction in temperature from reducing the laser power.

Where temperatures above 200 °C were observed, this seems to correlate with increased absorption at the laser wavelength and to small particle size. The large differences in laser heating among silicon carbide and ruby particles mentioned above is almost certainly related to variations in the amount of laser absorption, due to differences both in their dimensions or in the composition of individual particles. More surprising however is a calcite particle fired into aerogel whose Raman spectrum is shown in Figure 12. The Raman spectra of the other calcite particles which have been examined in aerogel are those of calcite at room temperature (Figure 2). But for this particle the spectrum is characteristic of calcite at a high temperature, showing the band broadening and shifts to lower wavenumbers that have been reported previously, particularly of the lattice vibration (near 280 cm^{-1}) that have been reported as characteristic of calcite at a high temperature (Gillet et al. 1993). From the published data on the variation of the wavenumbers of

the calcite bands over the range 20 °C to just below the decomposition temperature of calcite near 800 °C (Gillet et al. 1993), the temperature of this calcite particle in the laser beam is estimated to be about 600 °C. This high temperature is surprising since pure calcite is colourless and is not expected to absorb at the wavelength of the laser, and it thus seems likely that this heating is due to the additional presence of other strongly absorbing material in this particle.

Of relevance to these temperature measurements are our experiments on volatile-rich, hydrous materials such the phyllosilicate serpentine, which have shown no apparent change in the Raman spectral properties when subjected to intense green laser irradiation for intervals as long as 2 hours. As the thermal decomposition of serpentine is well understood from experimental data, and occurs with the loss of water and creation of anhydrous silicates such as olivine at a temperature of 500 °C, it seems that this temperature was not reached during laser irradiation.

Analysis of micrometeoroids Captured In Low-Earth Orbit

The discussions thus far have focussed on the Raman spectroscopic analysis that has been applied to particles accelerated into aerogel targets using the LGG. With the important consideration of sample heating by the laser excitation discussed in the previous section, Raman spectroscopy has now been applied to micrometeoroids captured in low Earth orbit by the Orbital Debris Collector (ODC) experiment that used 20 kg m^{-3} density silica aerogel (Hörz *et al*., 2000). This is an important evaluation of the technique as cometary particle may exhibit more fragmentation during hypervelocity capture than is observed in the laboratory simulations. An individual impact event was recovered from one of the aerogel tiles that made up the ODC experiment using the methodology described in Westphal *et al*., (2003). The impact event was suspected to be part of the chondritic swarm event that has been identified in the exposed tiles (Hörz *et al*., 2000) and therefore natural in origin rather than artificial orbital debris. Previous work using synchrotron based analysis techniques (e.g. Borg *et al*., 2004) have identified that the preserved impact events in the aerogel show extensive fragmentation along the length of the track. A required capability of any technique that analyses the particle while still encapsulated in aerogel is the ability to rapidly locate significant projectile material. It has already been shown that detail Raman maps can be acquired however these typically take in the order of 3-4 hours to completely map a significant area of track debris. A further complication is the formation of micron and sub-micron sized condensed aerogel fragments as a result of the hypervelocity collision that are intimately associated with the project debris and extremely difficult to discriminate against using just reflected or transmitted light (Figure 13a). It is therefore necessary to have the ability to pre-screen and area of interest.

Prior to the acquisition of Raman spectra, the terminal area of the impact event was subjected to fluorescence imaging at Lawrence Livermore National Laboratory using a 488 nm Ar^+ laser to excite the material. The laser beam was directed through a narrow bandpass filter to remove residual laser plasma lines, and was then coupled into the rear entrance port of the microscope. A pellicle beamsplitter partially reflected the laser beam to a ×100 magnification objective lens that focused the light to a nearly diffraction-limited spot (~500 nm) at the sample surface. The light emitted from the sample was focussed onto a pinhole with a 100 μm diameter by the microscope tube lens; this pinhole serves as the confocal aperture and reduces contributions from portions of the sample not in the focal volume. After passing through the pinhole, the light was collimated by a single antireflection-coated lens and passed through a holographic notch filter to attenuate the Rayleigh scattering. The remaining fluorescence was then focused onto a single photon counting avalanche photodiode (EG & G, model SPCM-AQR-14). Fluorescence images of the fragments in the aerogel were generated by raster-scanning the sample through the focused laser spot, as illustrated in Figure 13b and c. The extent to which the substrate aerogel can be modified by hypervelocity capture is illustrated by the cusp that partially surrounds the terminal grain; it is most likely that this observed feature is aerogel rather than projectile material (Figure

13c). Significantly the acquisition time for the fluorescence images is only a few minutes compared to the few hours for the Raman maps acquired for the Allende grain. From the areas of interest identified in the fluorescence images, the stage was used to centre these areas onto the excitation beam. The Raman scattered light was focused through the entrance slit of a 0.3 m monochromator (Acton SpectraPro 300i) that dispersed the light onto a liquid-nitrogen-cooled, back-thinned CCD camera (Roper Scientific LN/CCD-1340/100). Light dispersion was achieved by a 1200 groove/mm grating (λ_b = 500 nm), and the spectra were calibrated against a toluene standard. Typical incident laser powers were 200 μW, and integration times ranged from 2-6 min. Spectra collected from regions free of particles indicated a weak, broad fluorescent background across the wavelength range of interest. This weak background underlying the Raman spectra was removed by a polynomial fit (Figure 13d). The Raman spectroscopy identified that the material observed in the Figure 13b, was actually condensed aerogel material and not micrometeoroid debris. The Raman spectroscopic analysis of the terminal grain (Figure 13c-d) failed to identify any mineralogical components; however, these components may only exist as a nanometre-sized grains as in IDPs (e.g. Bradley, 2004), so further work on the size limitation capabilities of Raman spectroscopy must be investigated. Despite the lack of mineralogy data, the analysis identified peaks at 1357 cm^{-1} and 1596 cm^{-1} that correspond to the first order G- (*graphite*) and D- (*disorder*) bands, or simply referred to as carbonaceous material that have previous been identified in IDPs (e.g. Wopenka, 1988 and Raynal *et al*., 2000). The identification of carbonaceous material is significant as it would suggest that even at encounter velocities typically >10 km s^{-1}, organic material does survive capture and, more importantly, survives within intact grains rather than being deposited along the entire length of the impact event. This means that it maybe possible to distinguish between indigenous carbon and organic contamination that is present with the aerogel.

Extraction of particles from aerogel

The benefits of Raman spectroscopy are that as well as obtaining a chemical signature, the work can be done in-situ. However, for completeness we briefly discuss extraction of captured particles from aerogel. Extraction is discussed in detail in Westphal *et al*., 2002 and 2003, where sophisticated tools (silicon micro-tweezers) are used to extract particles. Here we note that for particles of large size (e.g. 50 microns or more across), such sophistication was not necessary. We used a simple drill (drill bit diameter 1.2 mm) to cut into the aerogel. Then standard fine metal tweezers were used to remove particles of 300 microns size. For particles of 100 microns dia., standard medical quality tools (e.g. surgical metal pick with a sticky end) were used to work particles free. Success at extraction was 100% after a training period that required test extraction of just 3 particles. We note that typical 106 micron dia. glass particles emerged from the aerogel with no attendant aerogel wrap. When examined under a SEM, as well as a lack of any indication of a wrap of molten aerogel being formed during capture, no fine surface damage was evident as compared to an un-shot glass bead.

At 50 microns particle size, particles could not be cleanly extracted with this method. Instead it was possible to remove the particle embedded in a near equal size block of aerogel. Note that when examined under a microscope, although an example such particle was in a block of aerogel, it again did not appear to have a wrap of molten aerogel set around it. This size appears to be the lower limit that can be extracted in this fashion. This indicates that for smaller sizes (i.e. the majority of particles expected in the Stardust aerogels), the methods of Westphal *et al*., 2002 and 2003 will be necessary to obtain extraction.

Conclusions

There are a variety of techniques for study of small particles from space (see Zolensky *et al*., 2000). For the particular case of particles captured in aerogel, the results of an extensive study are reported here. The use of Raman techniques (first demonstrated by Burchell *et al*., 2001) has now

been shown to be successful in identifying a wide range of minerals after their capture in aerogel at speeds of 5 to 6 km s^{1}. In some cases, fluorescent spectra have been obtained which are similarly useful in aiding identification. It is clear that success is not limited to just a few mineral types, but encompasses a wide range, and includes many of interest to planetary science. The laser spot size used was small (of the order of 5 microns across) and in some cases the particles illuminated were equally small. This suggests Raman techniques are well suited to the size ranges of coarser particles expected to be found in the Stardust aerogels. Further, Raman mapping of inhomogeneous particles (from Allende and Orgueil meteorites) can be carried out in-situ in the aerogel. This is shown to be a sensitive tool for particle study at small size scales, although not all the samples used (e.g. Murchison) gave strong signals.

In addition to this a study has been carried out of the heating effects on particles in aerogel during the laser illumination necessary for Raman study. Elevated temperatures were obtained. In the main, usable Raman spectra can be obtained for modest elevations in temperatures. Extreme temperatures can however also be obtained. Caution is thus advised and this suggests use of the lowest laser power on the sample compatible with obtaining a Raman spectrum.

Finally, an example of the use of Raman spectroscopy in analysing a dust particle captured in aerogel in space was given. Of particular interest is that sufficient of the particle remained intact at the end of the track for an analysis to be undertaken.

Overall, Raman spectroscopy is increasingly emerging as a powerful tool for study of extraterrestrial samples captured in aerogel. The return to Earth of the Stardust mission aerogel in 2006 will be keenly awaited. The 2800±500 particles bigger than 15 microns that are predicted to have impacted that aerogel (Tuzzolino *et al.*, 2004) at 6.1 km s^{-1} will be an invaluable resource for analysis. Provided intact particles exist at the ends of tracks, or fragments of greater than a few microns line the track walls, the material will be suitable for study by Raman techniques.

Acknowledgements

We thank M. Cole for the firing of the light gas gun; the Particle Physics and Astronomy Research Council (UK) for financial support. The research carried out by G. Graham and A. Esposito was performed under the auspices of the U.S. Department of Energy, National Nuclear Security Administration by the University of California, Lawrence Livermore National Laboratory under contract no. W-7405-Eng-48. We thank F. Hörz for supply of the piece of aerogel from the Orbital Debris Collector.

References

Amari S., Nittler L. R., Zinner E., Gallino R., Lugaro M. and Lewis, R. S. 2001 Presolar SiC grains of Type Y: Origin from Low-Metallicity Asymptotic Giant Branch Stars. *The Astrophysical Journal*, **546**; 248-266.

Bernatowicz T., Fraundorf G., Tang M., Anders E., Wopenka B., Zinner E. and Fraundorf P. 1987 Evidence for interstellar SiC in the Murray carbonaceous meteorite. *Nature* **330**; 728.

Borg J., Djouadi Z., Majtrajt G., Martinez-Criado G., Snead C.J., Somogyi A. and Westphal A.J. 2004. In-situ analyses of Earth orbital grains trapped in aerogel using synchrotron X-ray microfluorescence techniques (abstract #1580). 35th Lunar and Planetary Science Conference. CD-ROM.

Bradley, J. 2003. The Astromineralogy of Interplanetary Dust Particles. *Lecture Notes in Physics*, **609**; 217-235.

Bradley J.P. 2004. Interplanetary dust particles. In *Treatise of Geochemistry*, edited by Davies A.M., Holland H.D. and Turekian K.K. Amsterdam: Elsevier. Vol. 1., p689-711.

Brownlee D. E., Horz F., Hrubsch L., McDonnell J. A. M., Tsou P. and Williams J. 1994. Eureka !!. Aerogel Capture of Meteoroids in Space (abstract). *Lunar Planet Sci*. **25**; 183 – 184.

Brownlee D.E., Tsou P., Atkins K.L., Yen C.-W., Villinga J.M., Price S., and Clark B.C. 1996. STARDUST: Finessing expensive cometary sample returns. *Acta Astronautica*, **39**; 1-4, 51-60.

Brownlee D. E., Tsou P., Anderson J.D., Hanner M.S., Newburn R.L., Sekanina Z., Clark B.C., Hörz F., Zolensky M.E., Kissel J., McDonnell J.A.M., Sandford S.A., and Tuzzolino A.J. 2003. *J. Geophys. Res. (Planets)* **108**(E10); 8111.

Burchell M. J., Thomson R., and Yano H. 1999a. Capture of Hypervelocity Particles in Aerogel; In Ground Laboratory and Low Earth Orbit, *Planetary and Space Science* **47**; 189 – 204.

Burchell M. J., Cole M.J., McDonnell J.A.M., and Zarnecki J.C. 1999b. Hypervelocity Impact Studies Using the 2 MV Van de Graaff Accelerator and Two-Stage Light Gas Gun of the University of Kent at Canterbury. *Meas. Sci. Technol*. **10**; 41 – 50.

Burchell M. J., Creighton J.A., Cole M.J., Mann J., and Kearsley A.T. 2001. Capture of particles in hypervelocity impacts in aerogel. *Meteoritics and Planetary Science* **36**; 209 – 221.

Burchell M. J., Creighton J.A., and Kearsley A.T. 2004. Identification of organic particles via Raman techniques after capture in hypervelocity impacts on aerogel. *Journal of Raman Spectroscopy* **35**; 249 – 253.

Crovisier, J., Leech, K., Bockelee-Morvan, D., Brooke, T.Y., Hanner, M.S., Altieri, B., Keller, H.U. and Lellouch, E. 1997 The spectrum of Comet Hale-Bopp (C/1995 01) observed with the Infrared Space Observatory at 2.9 AU from the Sun. *Science*, **275**; 1904-1907.

Delaney J.S. 1989. Lunar Basalt Breccia Identified among Antarctic Meteorites. *Nature* **342**; 889 – 890.

Edwards H. G. M., Farwell D.W., Grady M.M., Wynn-Williams D.D., and Wright I.P. 1999. Comparative Raman Microscopy of a Martian Meteorite and Antarctic Lithic Analogues. *Planetary and Space Science* **47**; 353 – 362.

Fagan T. J., Scott E.R.D., Keil K., Cooney T.F., and Sharma S.K. 2000. Formation of Feldspathic and Metallic Melts in Shock Enstatite Chondrite Reckling Peak A80259. *Meteoritics and Planetary Science* **35**; 319 – 329.

Flynn G. J., Horz F., Bajt S., and Sutton S.R. 1996. In-situ chemical analysis of extraterrestrial material captured in aerogel. *Lunar and Planet. Sci. Conf*. **XXVII**; 396-370.

Fujiwara A., Mukai T., Kawaguchi J., and Useugi K.T. 1999. Sample Return Missions to Small Bodies. *Advances in Space Research* **25**; 231 – 238.

Fujiwara, A., Abe, M., Kato, M., Kushiro, I., Mukai, T., Okada, T., Saito, J., Sasaki, S., Yano, H. and Yeoman, D. 2004 Sample return science by Hayabusa near-Earth Asteroid Mission (abstract). Lunar and Planetary Science Conference XXXV. Abstract #1521.

Gaffey M. J. (1999) Bias correction of the relative fluxes of the meteorite types: asteroid spectroscopy and orbital dynamics. *Meteorit. Planet. Sci*., **35**; A57-58.

Gillet P., Biellmann C., Reynard B., and McMillan P. 1993. Raman spectroscopic studies of carbonates Part I: high-pressure and high temperature behaviour of calcite, magnesite, dolomite and aragonite. *Phys. Chem. Minerals* **20**; 1-18

Gounelle, M. and Zolensky, M.E. 2001 A terrestrial origin for sulfate veins in CI1 chondrites (abstract) Lunar and Planetary Science Conference XXXII abstract #1609.

Graham, G.A., Kearsley, A.T., Wright, I.P., Grady, M.M., Drolshagen, G., McBride, N.M., Green, S.F., Burchell, M.J., Yano, H. & Elliott, R. 2001a Analysis of Impact Residues on Spacecraft Surfaces: Possibilities and Problems, *In: Proceedings of the Third European Conference on Space Debris*, ESA Special Publication 473; 197-203.

Graham G. A., Franchi I.A., Kearsley A.T., and Burchell M.J. 2001b. The Use of a Raman Microprobe in Analysis of Extraterrestrial Material Impacted into Aerogel. *Proceedings of the Royal Microscopial Society* **36**; 251 – 254.

Graham, G. A., Kearsley, A. T., Butterworth, A.L., Bland, P.A., Burchell, M.J., McPhail, D. S., Chater, R. J., Grady, M.M., and Wright, I.P. 2004 Extraction and microanalysis of cosmic dust collected during sample return missions: Laboratory simulations. *Advances in Space Research,* in press.

Greenberg, J.M. and Hage, J.I. 1990 From Interstellar dust to Comets: A Unification of Observational Constraints. *Astrophysical Journal* **361**; 260-274.

Heide F., and Wlotzka F. 1995. Meteorites: Messengers from Space. Pub. Springer-Verlag, Berlin.

Heymann D. 1987. Raman spectra of carbon in the Canyon Diablo iron meteorite. *Lunar and Planet. Sci. Conf*. **XVIII**; 419 – 420.

Hörz F., Zolensky M.E., Bernhard R.P., See T.H., and Warren J.L. 2000. Impact Features and Projectile Residues in Aerogel Exposed on Mir, *Icarus* **147**; 559 – 579.

Jones A.P., Claeys P., and Heuschkel S. 2000 Impact melting of carbonates from the Chicxulub impact crater. In Gilmour, I. and Koeberl, C. (eds) Impacts and the Early Earth. *Lecture Notes in Earth Sciences* **91**; 343-361.

Kawaguchi J., Useugi K., and Fujiwara A. 2003. The MUSES-C mission for the sample and return – its technology development status and readiness. *Acta Asronautica* **52**; 117 – 123.

McCumber D. E., and Sturge M.D. 1963. Linewidth and temperature shift of the R lines in ruby. *J. Appl. Phys*., **34**; 1682-1684.]

Michel-Levy M. C., and Lautie A. 1981. Microanalysis by Raman spectroscopy of carbon in chondrites. *Meteoritics* **16**; 301 – 302.

Müller W. F., Weinbruch S., Walter R., and Müller-Beneke G. 1995. Transmission Electron Microscopy of Chondrule Minerals in the Allende Meteorites: Constraints on the Thermal and Deformational History of Granular Olivine-Pyroxene Chondrules. *Planetary and Space Science* **43**; 469 – 483.

Murakami T., and Ikeda Y. 1994. Petrology and Mineralogy of the Yamato 86751 CV3 Chondrite. *Meteoritics and Planetary Science* **29**; 397 – 408.

Popp J., Tarcea N., Keifer W., Hilchenbach M., Thomas N., Stuffler T., Hofer S., Stöffler D., and Greshake A. 2002. The effect of surface texture on the mineralogical analysis of chondritic meteorites using Raman spectroscopy. *Planetary and Space Science* **50**; 865 – 870.

Sautter V., Barrat J.A., Jambon A., Lorand J.P., Gillet P., Javoy M., Joron J.L., and Lesourd M. 2002. A New Martian Meteorites from Morocco: The Nakhlite North West Africa 817. *Earth and Planetary Science Letters* **195**; 223 – 238.

Raynal P.I., Quirico E., Borg J. and d'Hendecourt L. 2000. Micro-Raman study of the carbon phase in 6 IDPs (abstract #1318). 31st Lunar and Planetary Science Conference. CD-ROM.

Tsou P., Brownlee D.E., Laurance M.R., Hrubesh L., and Albee A.L. 1988. Intact capture of hypervelocity micrometeoroid analogs (abstract). *Lunar Planet Sci. Conf*. **19**; 1205 – 1206.

Tsou P., Brownlee D.E., Sandford S.A., Hörz F., Zolensky M.E. 2003. Wild-2 and interstellar sample collection and Earth return. *J. Geophys. Res. (Planets)* **108**(E10); 8113.

Tuzzolino A. J., Economou T.E., Clark B.C., Tsou P., Brownlee D.E., Green S.F., McDonnell J.A.M., and Colwell M.T.S.H. 2004. Dust Measurements in the Coma of Comet 81P/Wild2 by the Dust Flux Monitor Instrument. *Science* **304**; 1776 – 1780.

Wang A., Jolliff B.L., Haskin L.A. 1999. Raman spectroscopic characterisation of a Martian SNC meteorites: Zagami. *J. Geophys. Res. (Planets)* **104**(E4); 8509 – 8519.

Westphal A. J., Snead C., Borg J., Quirico E., Raynal P.-I., Zolensky M.E., G. Ferrini G., Colangeli L., and Palumbo P. 2002. Small hypervelocity particles captured in aerogel collectors: Location, extraction, handling and storage. *Meteoritics and Planetary Science* **37**; 855 – 865.

Westphal A.J., Snead C., Dominguez G., Bradley J.P., Zolensky M.E., Flynn G. and Brownlee D. 2003. An extraction and curation technique for particles captured in aerogel collectors (abstract #1826). 34st Lunar and Planetary Science Conference. CD-ROM.

Wopenka B. 1988. Raman observations on individual interplanetary dust particles. *Earth Planet. Sci. Lett*. **88**; 221 – 231.

Wopenka B. and Sandford S.A. 1984. Laser Raman microprobe study of mineral phases in meteorites. *Meteoritics* **19**; 340 – 341.

Wynn-Williams D. D., and Edwards H.G.M. 2000. Proximal Analysis of Regolith Habitats and Protective Biomolecules in Situ by Laser Raman Spectroscopy: Overview of terrestrial Antarctic Habitats and Mars Analogs. *Icarus* **144**; 486 – 503.

Zolensky M. E., Pieters C., Clark B., and Papike J.J. 2000. Small is beautiful: The analysis of nanogram-sized astromaterials. *Meteoritics and Planetary Science* **35**; 9 – 29.

Tables

Table 1: Minerals used in the Raman studies.

Mineral	Aerogel density (kg m^{-3})	Impact speed (km s^{-1})	Chemical Formula	Example Meteoritic Types[1]	References
Albite	110	4.5	$NaAlSi_3O_8$	Ach, Ch, Mes	Heide & Wlotzka, 1995
				North West Africa 817	Sautter *et al*., 2002
Calcite	110	4.2	$CaCO_3$	cCh	Heide & Wlotzka, 1995
				Nakhla	Edwards *et al*., 1999
Corundum (ruby)	96	4.95	Al_2O_3	Allende	Müller *et al*., 1995
Enstatite (Pyroxene)	96	4.80	$MgSiO_3$	Ach, Ch, Mes	Heide & Wlotzka, 1995
				Yamato 86751	Murakami & Ikeda, 1994
				Reckling Peak A80259	Fagan *et al*., 2000
Lizardite	60	5.1	$Mg_3Si_2O_5(OH)_4$	cCh	Heide & Wlotzka, 1995
Nepheline	110	5.7	$NaAlSiO_4$	cCh	Heide & Wlotzka, 1995
				Allende	Müller *et al*., 1995
				Yamato 86751	Murakami & Ikeda, 1994
Olivine	96	5.1	$(Mg,Fe)_2SiO_4$	Ch, Pal, Mes, Ach	Heide & Wlotzka, 1995
				Elephant Moraine 87521	Delaney, 1989
				Allende	Müller *et al*., 1995
Diopside (Pyroxene)	96	5.1	$(CaMg)SiO_3$	Ch, Pal, Mes, Ach	Heide & Wlotzka, 1995
				Elephant Moraine 87521	Delaney, 1989
				Allende	Müller *et al*., 1995
Rhodonite	60	5.1	$MnSiO_3$	Ch	Heide & Wlotzka, 1995
Serpentine	110	No impacts	$Mg_3Si_2O_5(OH)_4$	cCh	Heide & Wlotzka, 1995
				Allende	Müller *et al*., 1995
Spinel	96	4.95	$MgAl_2O_4$	Ch, cCh	Heide & Wlotzka, 1995
				Allende	Müller *et al*., 1995
				Yamato 86751	Murakami & Ikeda, 1994

1 Ach = Acondritic meteorites, Ch = chondrites, cCH = Carbonaceous chondrites, Pal = Pallasites, Mes = Mesosiderites. In some case specific examples of meteorites are given.

Table 2. Minerals identified in meteorite grains as determined from Raman spectra

Meteorite	**Composition from Raman spectra**
Murchison	Magnesite/dolomite
	Olivine
	Enstatite
Orgueil	Barite
	Jarosite
	Sulfur
	Hematite
	Albite
Allende	Olivine
	Diopside (pyroxene)

Figures

Figure 1. Typical track in aerogel (side view). An impact of Rhodonite in aerogel (density 60 kg m^{-3}) at 5.1 km s^{-1}. Track length 3.6 mm, particle size 54 microns. The impact was from the left, the particle position is marked with an arrow.

Figure 2. Raman spectra of mineral grains, showing in each case (upper trace) the spectrum of a grain trapped in aerogel and (lower trace) the raw grain spectrum.

Figure 3. Fluorescence spectra of alumina and spinel (raw grains and grains trapped in aerogel) excited by the helium neon laser. In each case the lower trace is the raw grain spectrum and the upper trace is from the grain captured in the aerogel. The spectral range shown corresponds to wavenumber shifts from the 632.8 nm laser line of 803 to 1475 cm^{-1}.

Figure 4. Three distinct fluorescence spectra observed from alumina samples, excited by the helium neon laser. The spectral range shown corresponds to wavenumber shifts from the 632.8 nm laser line of 200 to 2200 cm^{-1}.

Figure 5. Raman spectrum of silicon carbide grain in aerogel (top spectrum), and of a raw silicon carbide grain (bottom spectrum).

Figure 4. Top spectrum: various ruby particles in aerogel. Bottom spectrum, raw ruby grains

Figure 6. Raman spectra showing (upper trace) highly amorphous carbon in raw Murchison meteorite grains and (lower trace) less disordered carbon, with a structure closer to that of graphite, in Allende meteorite grains.

Figure 7. Raman spectra from raw meteorite samples (upper trace in each plot) matched with standard mineral spectra (lower trace). (a) and (b) Murchison meteorite showing a match for enstatite and anatase; (c) and (d) Allende showing a match for olivine and pyroxene; (e) and (f) Orgueil showing a match for sulphur and epsomite. The Allende meteorite spectra also show the presence of graphitic carbon (see Fig. 6).

Figure 8. (a) Raman spectrum (upper trace) from Allende meteorite sample captured in aerogel at 5 km s^{-1}, and (lower trace) a reference spectrum of olivine; (b) Raman spectrum (upper trace) from Orgueil meteorite sample captured in aerogel at 5 km s^{-1}, and (lower trace) a reference spectrum of pyroxene. In (b) the broad band at 1300-1600 cm^{-1} in the upper spectrum of indicates the presence also of amorphous carbon in the captured Orgueil particle.

Figure. 9. Allende grain in aerogel (a) white light illumination, and Raman maps at (b) 817 cm^{-1} (i.e. Olivine), (c) 851 cm^{-1}, (i.e. olivine), and (d) 1590 cm^{-1} (i.e. carbon peak).

Figure 10. (a) The Stokes and anti-Stokes Raman lines for a silicon carbide particle, T = 180 °C. (b) Raman spectra of a strongly absorbing particle (size 50 μm) trapped in aerogel on both the anti-Stokes and Stokes sides of the laser line, showing (upper trace) the effects of laser heating of the sample. The upper trace shows a spectrum recorded with a laser power of 2 mW at the sample, and the lower trace shows an identical run except that the laser power was reduced to 0.2 mW.

Figure 11. Fluorescence spectra from ruby particle in aerogel at 3 mW laser power (top spectrum), and (lower spectra) with an attenuated laser beam. The spectra have been scaled and shifted vertically for presentation.

Figure 12. Top spectrum: calcite particle in aerogel, showing band shifts and broadening consistent with laser heating to ca. 600 °C. Bottom spectrum: calcite at room temperature (from Lyon database).

Figure 13. (a) Transmitted light micrograph of a complete impact event preserved in aerogel extracted from a bulk collector tile of the ODC experiment. The insert identified material that is scattered along the length of the terminal portion of the event. (b-c) Fluorescence images of material located along and at the terminal point track that had been identified in the insert image in (a). (d) Raman spectrum acquired for the terminal particle containing disordered carbonaceous peaks at 1357 and 1596 cm^{-1}.

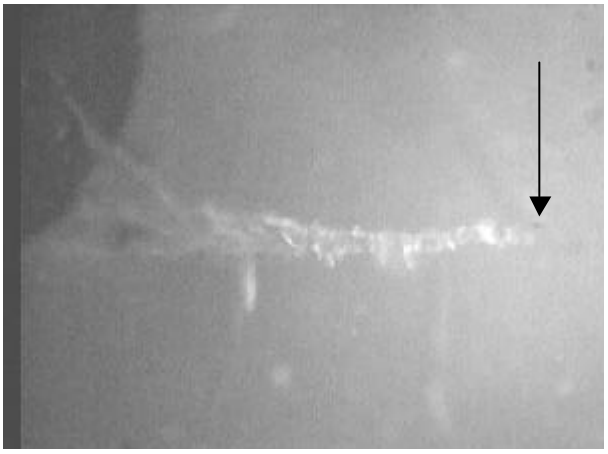

Figure 1. Typical track in aerogel (side view). An impact of Rhodonite in aerogel (density 60 kg m^{-3}) at 5.1 km s^{-1}. Track length 3.6 mm, particle size 54 microns. The impact was from the left, the particle position is marked with an arrow

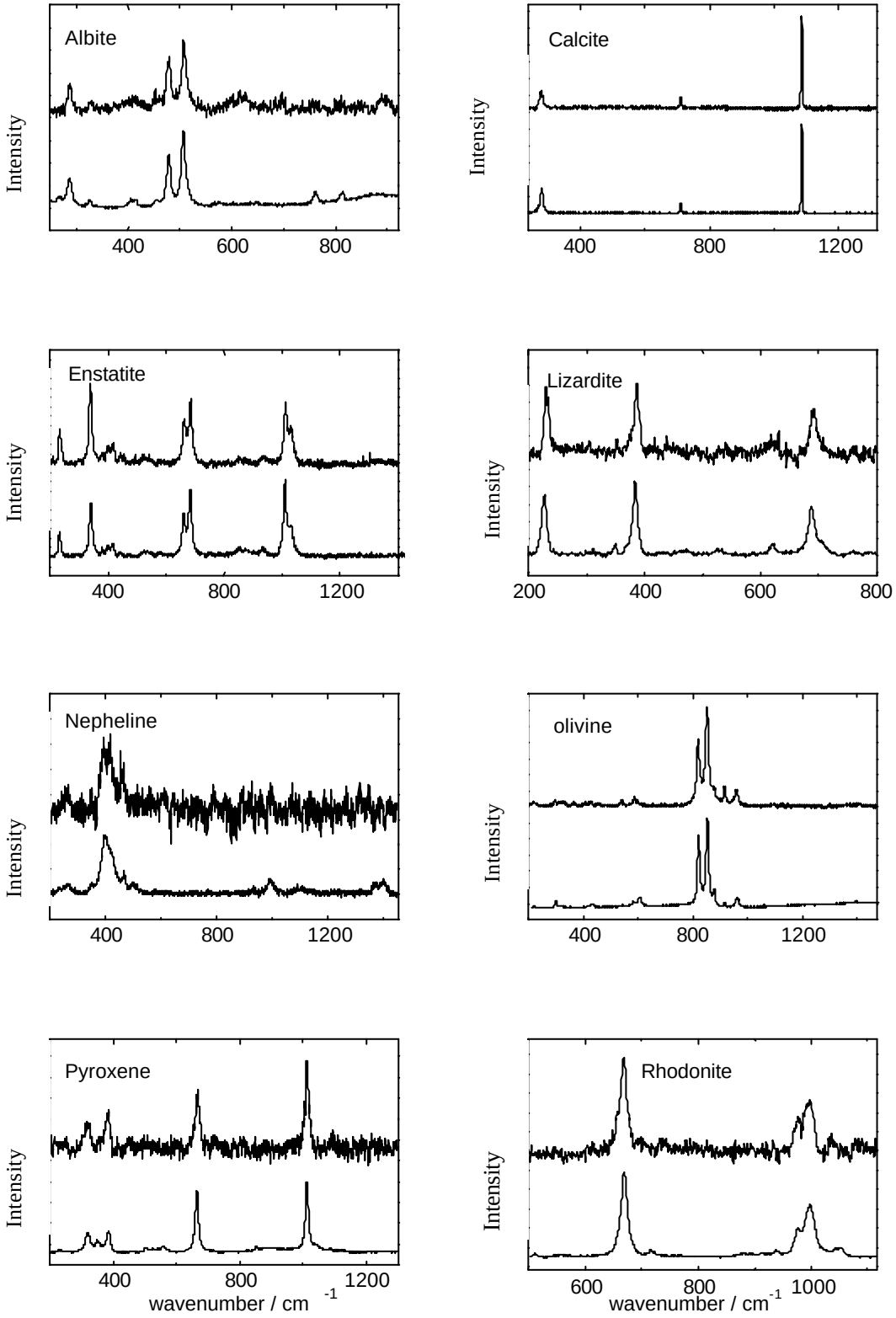

Figure 2. Raman spectra of mineral grains, showing in each case (upper trace) the spectrum of a grain trapped in aerogel and (lower trace) the raw grain spectrum.

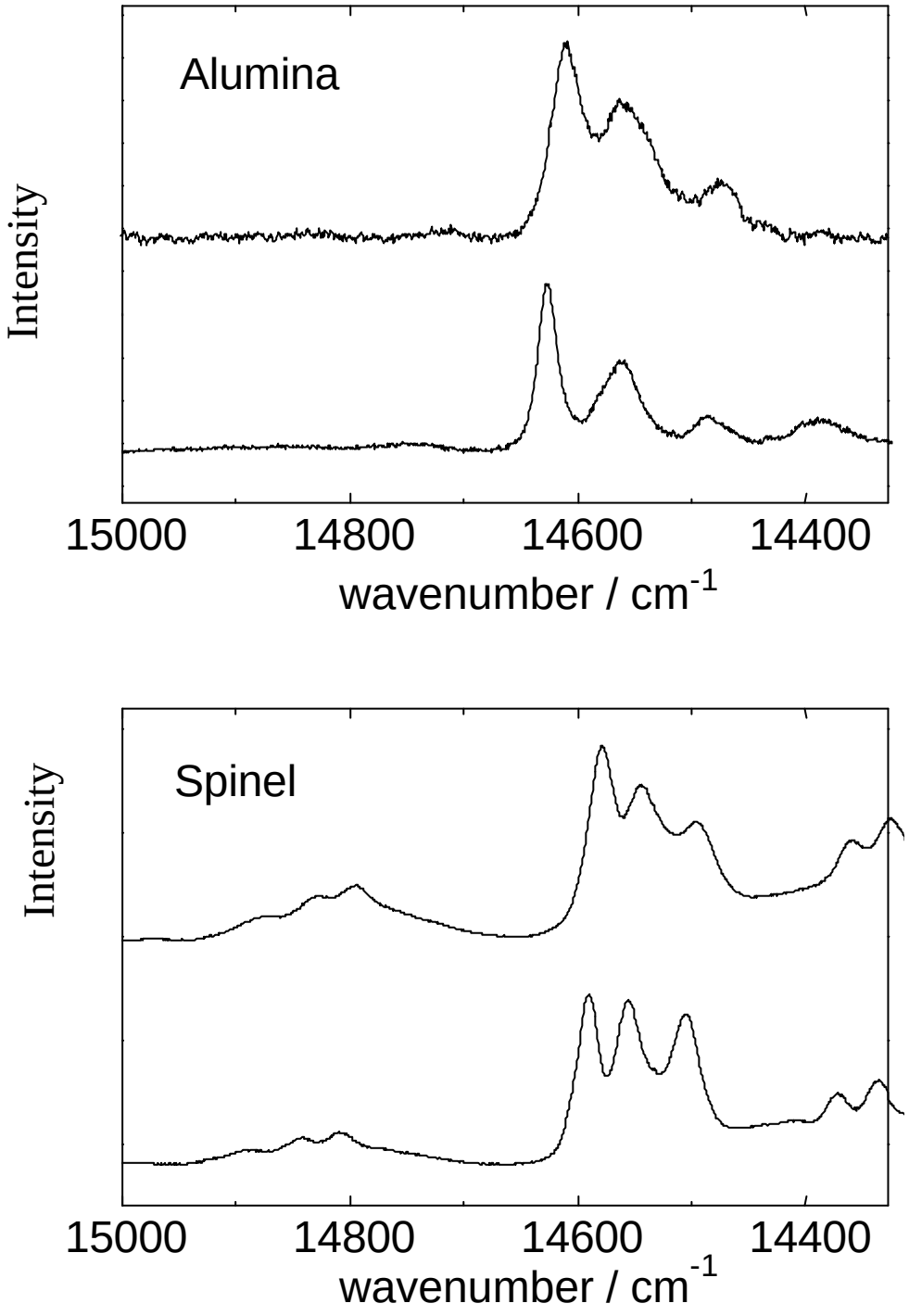

Figure 3. Fluorescence spectra of alumina and spinel (raw grains and grains trapped in aerogel) excited by the helium neon laser. In each case the lower trace is the raw grain spectrum and the upper trace is from the grain captured in the aerogel. The spectral range shown corresponds to wavenumber shifts from the 632.8 nm laser line of 803 to 1475 cm^{-1}.

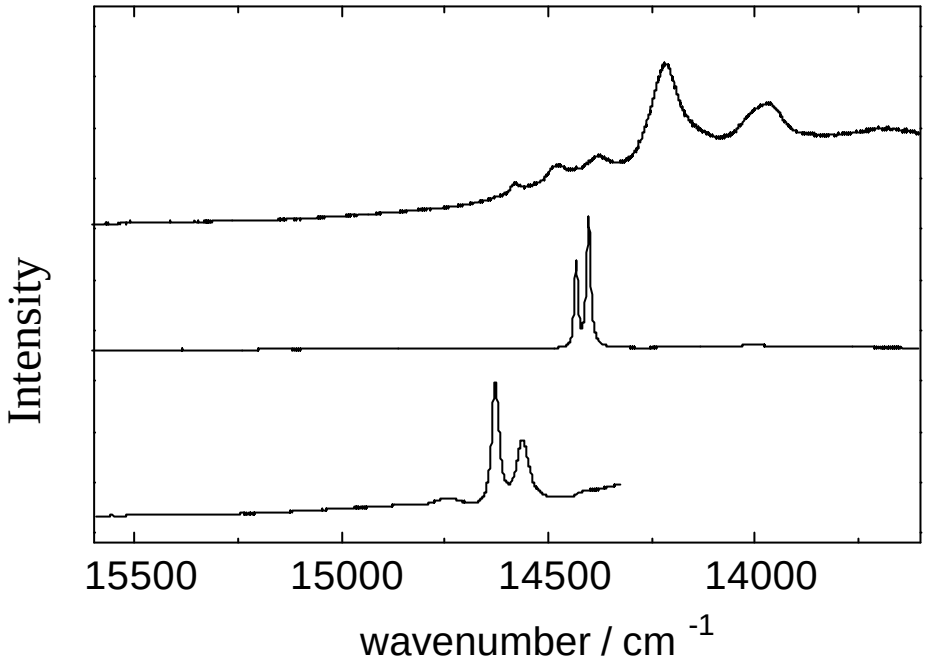

Figure 4. Three distinct fluorescence spectra observed from alumina samples, excited by the helium neon laser. The spectral range shown corresponds to wavenumber shifts from the 632.8 nm laser line of 200 to 2200 cm^{-1}.

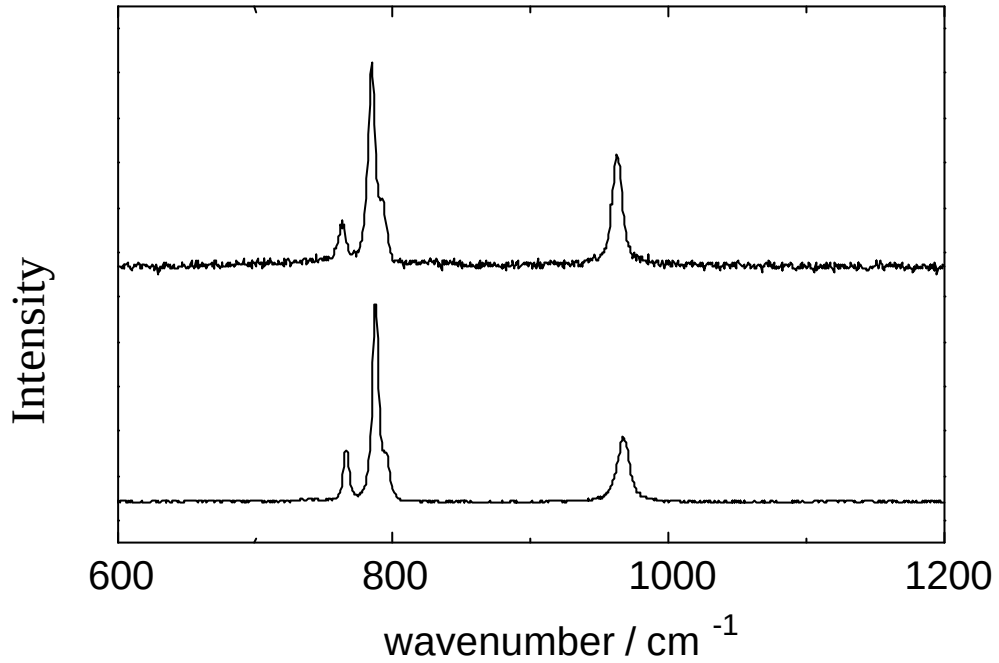

Fig 5. Raman spectrum of silicon carbide grain in aerogel (top spectrum), and of a raw silicon carbide grain (bottom spectrum).

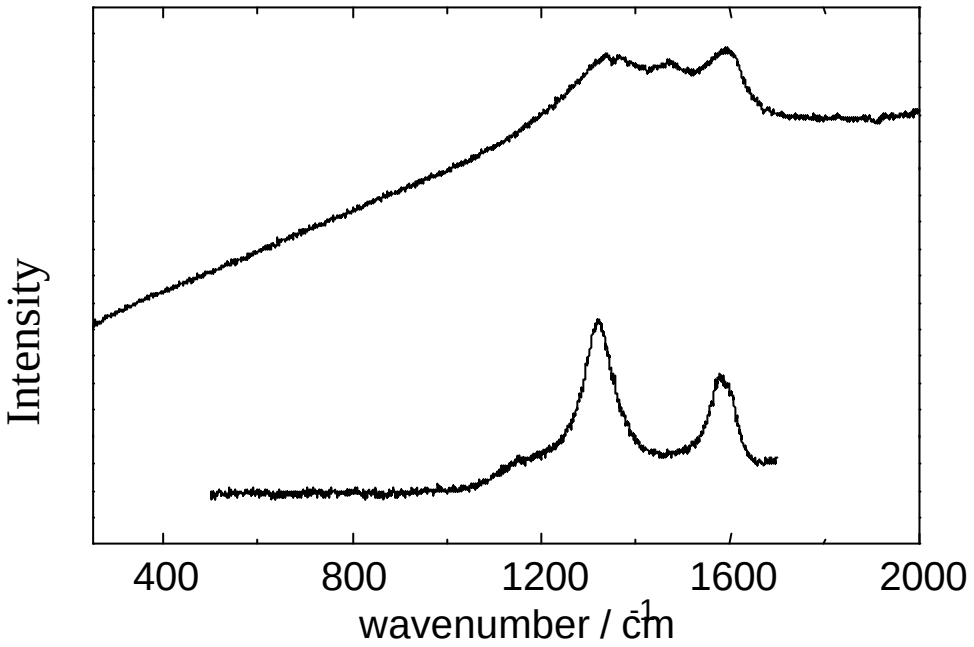

Figure 6. Raman spectra showing (upper trace) highly amorphous carbon in raw Murchison meteorite grains and (lower trace) less disordered carbon, with a structure closer to that of graphite, in Allende meteorite grains.

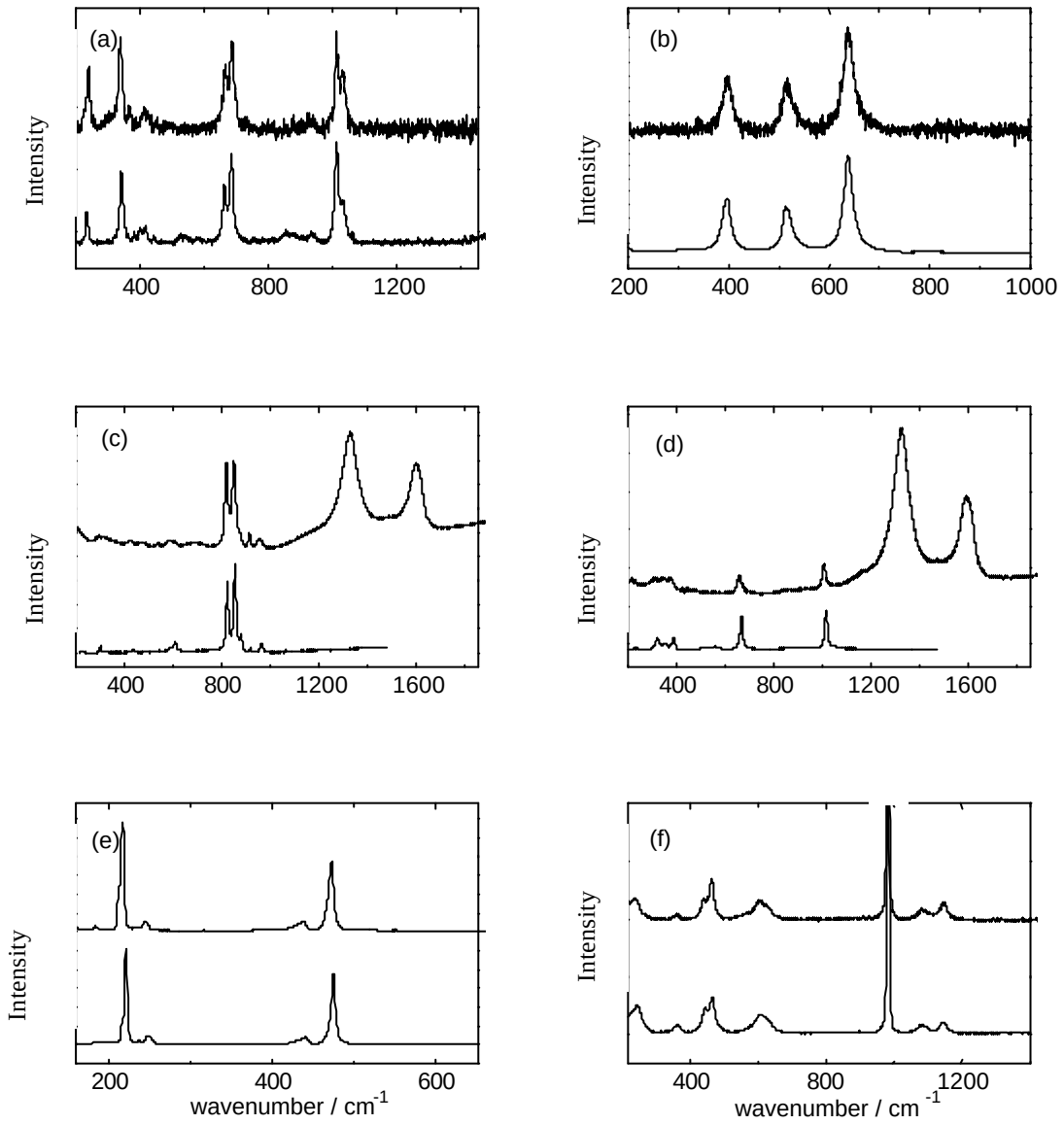

Figure 7. Raman spectra from raw meteorite samples (upper trace in each plot) matched with standard mineral spectra (lower trace). (a) and (b) Murchison meteorite showing a match for enstatite and anatase; (c) and (d) Allende showing a match for olivine and pyroxene; (e) and (f) Orgueil showing a match for sulphur and epsomite. The Allende meteorite spectra also show the presence of graphitic carbon (see Fig. 6).

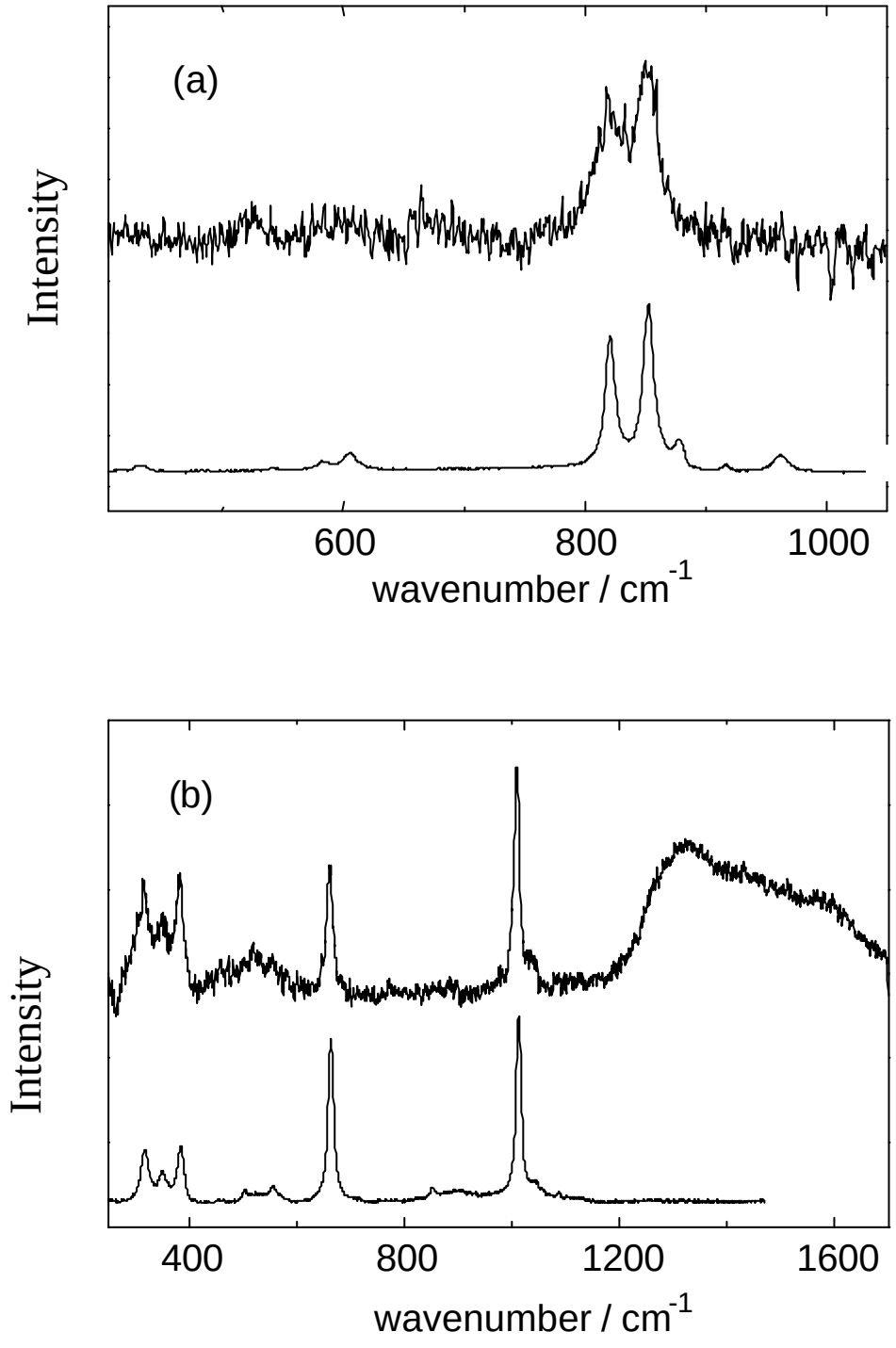

Figure 8. (a) Raman spectrum (upper trace) from Allende meteorite sample captured in aerogel at 5 km s^{-1}, and (lower trace) a reference spectrum of olivine; (b) Raman spectrum (upper trace) from Orgueil meteorite sample captured in aerogel at 5 km s^{-1}, and (lower trace) a reference spectrum of pyroxene. In (b) the broad band at 1300-1600 cm^{-1} in the upper spectrum of indicates the presence also of amorphous carbon in the captured Orgueil particle.

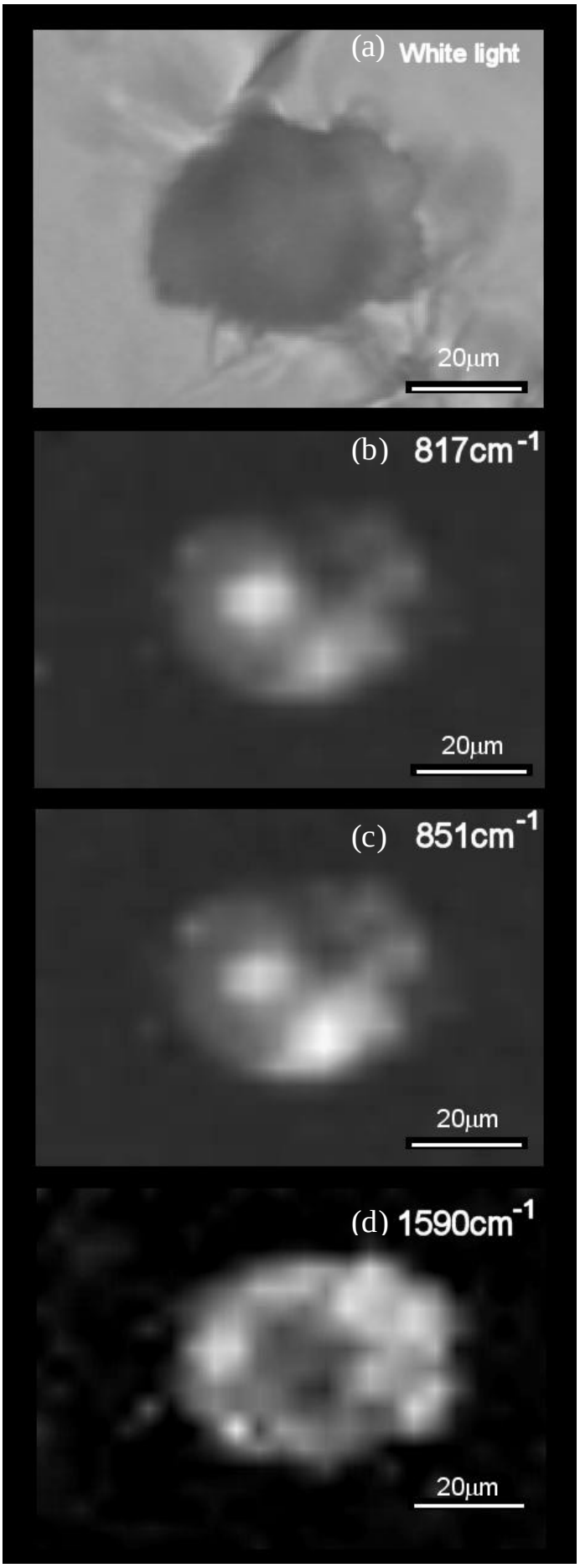

Figure. 9. Allende grain in aerogel (a) white light illumination, and Raman maps at (b) 817 cm^{-1} (i.e. Olivine), (c) 851 cm^{-1}, (i.e. olivine), and (d) 1590 cm^{-1} (i.e. carbon peak).

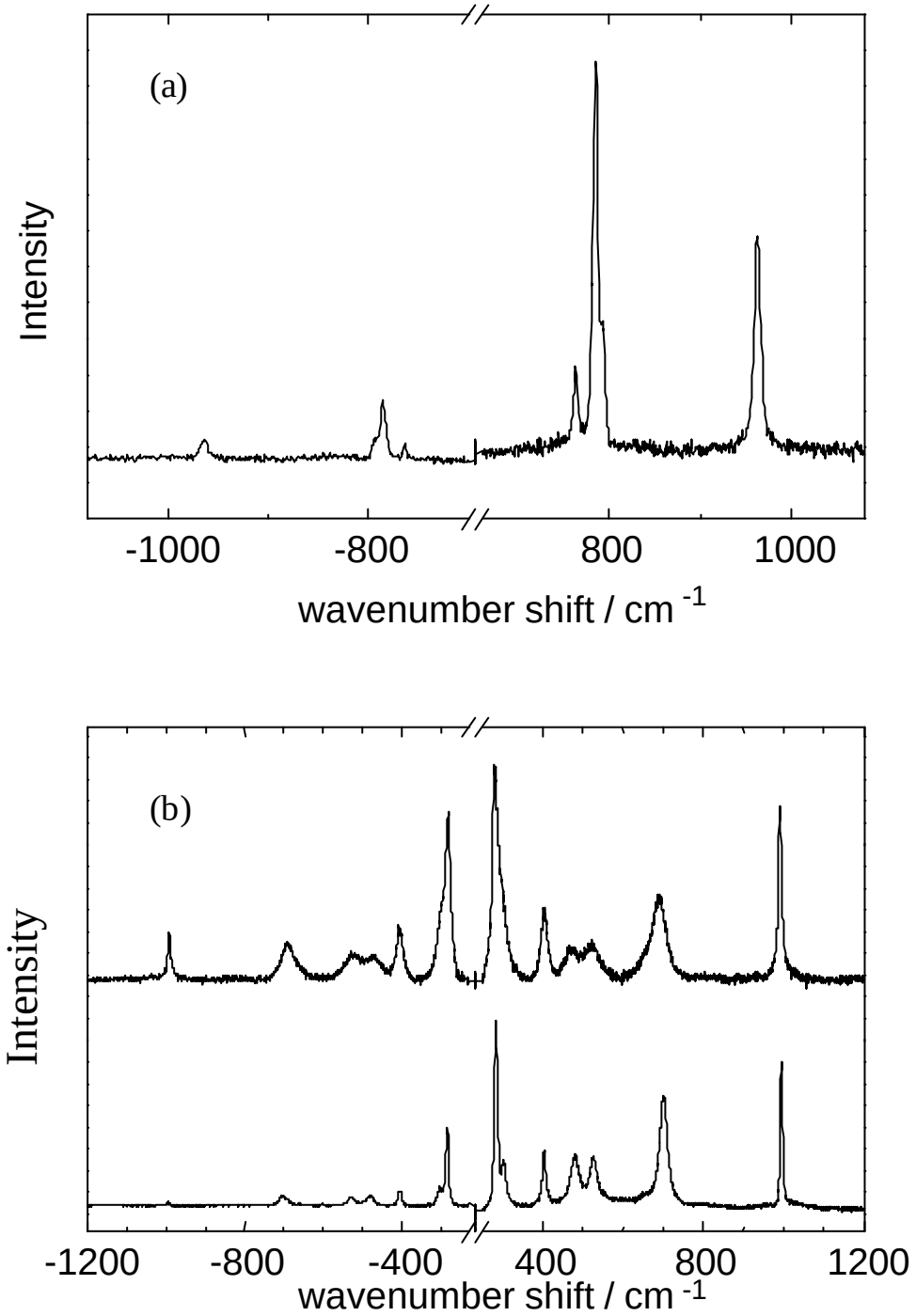

Figure 10. (a) The Stokes and anti-Stokes Raman lines for a silicon carbide particle, T = 180 °C. (b) Raman spectra of a strongly absorbing particle (size 50 μm) trapped in aerogel on both the anti-Stokes and Stokes sides of the laser line, showing (upper trace) the effects of laser heating of the sample. The upper trace shows a spectrum recorded with a laser power of 2 mW at the sample, and the lower trace shows an identical run except that the laser power was reduced to 0.2 mW.

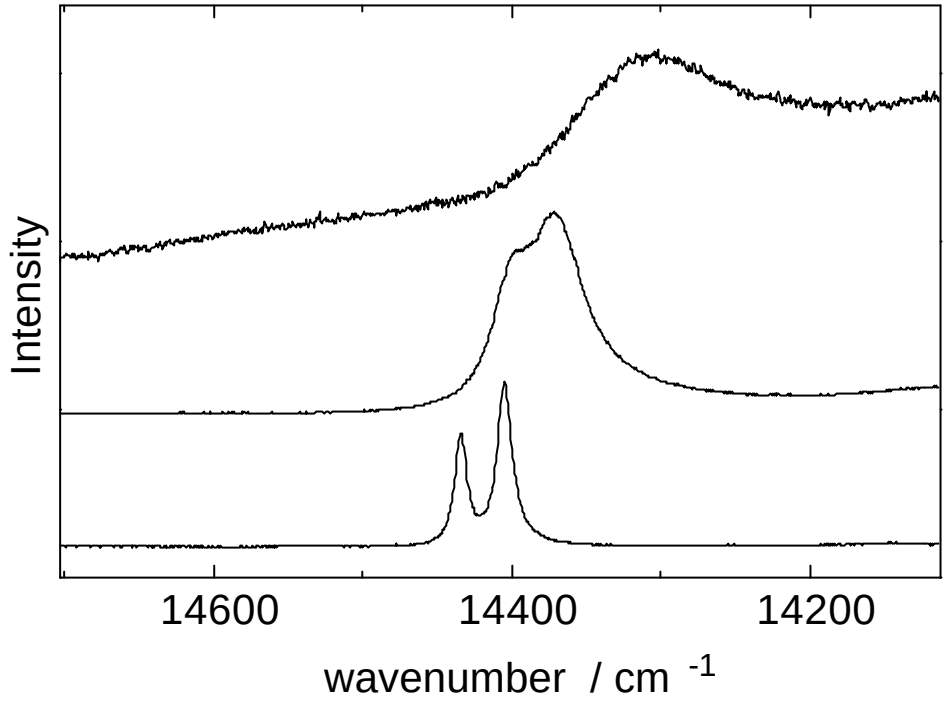

Figure 11. Fluorescence spectra from ruby particle in aerogel at 3 mW laser power (top spectrum), and (lower spectra) with an attenuated laser beam. The spectra have been scaled and shifted vertically for presentation.

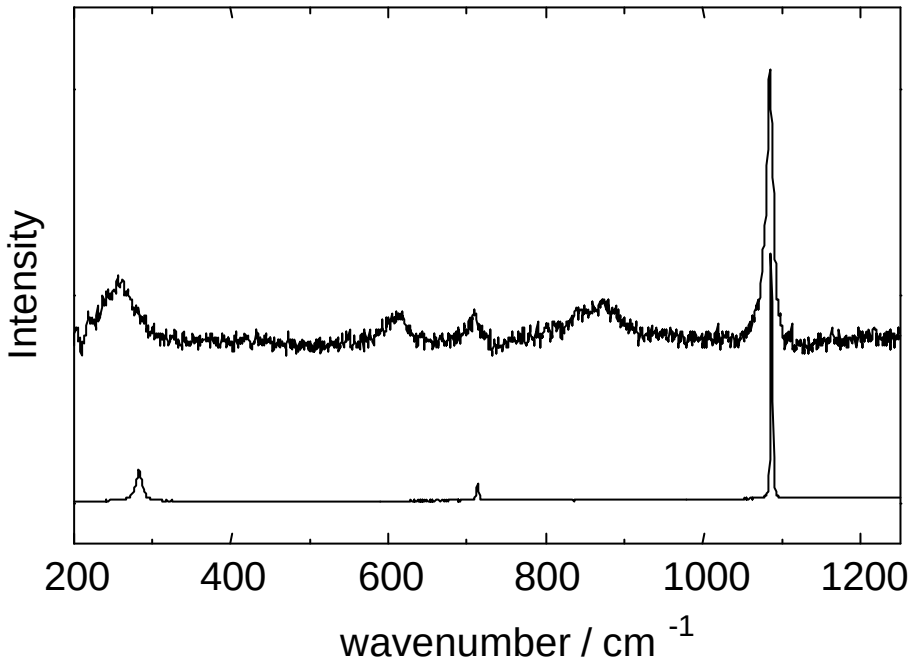

Figure 12. Top spectrum: calcite particle in aerogel, showing band shifts and broadening consistent with laser heating to ca. 600 °C. Bottom spectrum: calcite at room temperature (from Lyon database).

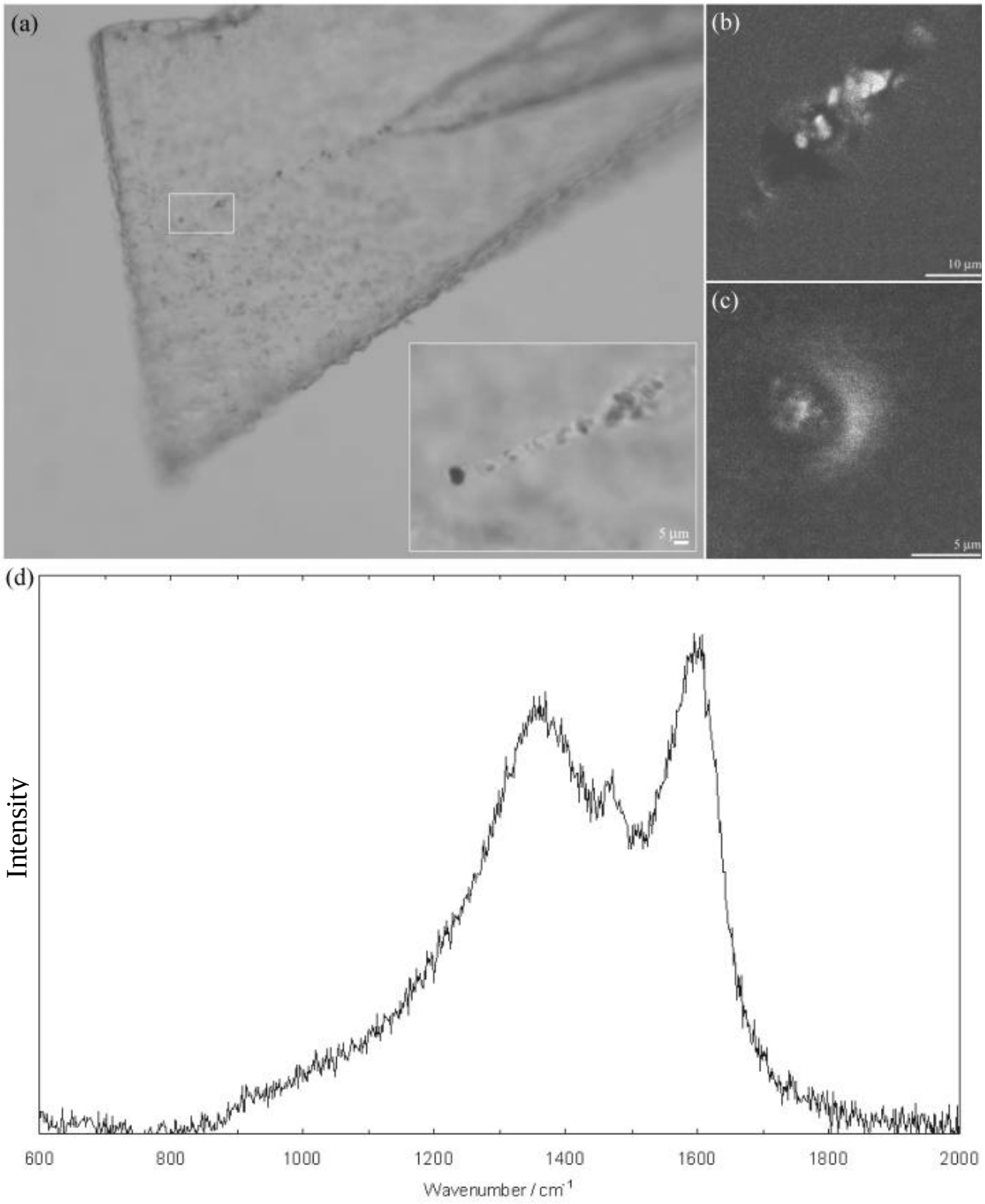

Figure 13. (a) Transmitted light micrograph of a complete impact event preserved in aerogel extracted from a bulk collector tile of the ODC experiment. The insert identified material that is scattered along the length of the terminal portion of the event. (b-c) Fluorescence images of material located along and at the terminal point track that had been identified in the insert image in (a). (d) Raman spectrum acquired for the terminal particle containing disordered carbonaceous peaks at 1357 and 1596 cm^{-1}.